# Surface effects on the dual-mode vibration of <110> silver nanowires with different cross-sections

*H.F. Zhan and Y.T. Gu**

*School of Chemistry, Physics and Mechanical Engineering, Queensland University of Technology, Brisbane 4001, Australia*

***Corresponding Author:** Dr. Yuantong Gu

**Mailing Address:** School of Chemistry, Physics and Mechanical Engineering,
Queensland University of Technology,
GPO Box 2434, Brisbane, QLD 4001, Australia

**Telephones:** +61-7-31381009

**Fax:** +61-7-31381469

**E-mail:** yuantong.gu@qut.edu.au

**Abstract:** Dual-mode vibration of nanowires has been reported experimentally through actuation of the nanowire at its resonance frequency, which is expected to open up a variety of new modalities for the NEMS that could operate in the nonlinear regime. In the present work, we utilize large scale molecular dynamics simulations to investigate the dual-mode vibration of <110> Ag nanowires with triangular, rhombic and truncated rhombic cross-sections. By incorporating the generalized Young-Laplace equation into Euler-Bernoulli beam theory, the influence of surface effects on the dual-mode vibration is studied. Due to the different lattice spacing in principal axes of inertia of the {110} atomic layers, the NW is also modeled as a discrete system to reveal the influence from such specific atomic arrangement. It is found that the <110> Ag NW will under a dual-mode vibration if the actuation direction is deviated from the two principal axes of inertia. The predictions of the two first mode natural frequencies by the classical beam model appear underestimated comparing with the MD results, which are found to be enhanced by the discrete model. Particularly, the predictions by the beam theory with the contribution of surface effects are uniformly larger than the classical beam model, which exhibit better agreement with MD results for larger cross-sectional size. However, for ultrathin NWs, current consideration of surface effects is still experiencing certain inaccuracy. In all, for all different cross-sections, the inclusion of surface effects is found to reduce the difference between the two first mode natural frequencies. This trend is observed consistent with MD results. This study provides a first comprehensive investigation on the dual-mode vibration of <110> oriented Ag NWs, which is supposed to benefit the applications of NWs that acting as a resonating beam.

**Keywords:** dual-mode vibration, nanowire, surface effects, natural frequency, beam theory

## 1. Introduction

Nanowires (NWs) exhibit extraordinary mechanical, electrical, optical and thermal properties, which enabled them being widely utilized as active components of nanoelectromechanical systems (NEMS) [1], such as high frequency resonators [2], field effect transistors (FETs) [3], nano switches [4], and other devices [5-7]. Specifically, NWs commonly play a role of a vibrating beam in NEMS, and very minute changes in the local environment, such as perturbations in forces, pressure or mass, can be detected by monitoring the corresponding changes in the resonance frequency of the NW [8]. Successful applications of this nanowire-based NEMS can be found in atomic force microscopy (AFM) and various kinds of sensors and actuators [7, 9]. Hence, it is crucial to characterize the vibrational properties of NWs.

Currently, great research efforts have been made to probe the vibrational properties of NWs. A number of experimental studies on the resonant frequencies of both metallic and semiconducting NWs can be found [10-17]. Using either surface-based extensions of continuum elasticity theory [18, 19] or multi-scale computational techniques [20-22], some researchers examined surface stress effects on the

resonant frequencies of NWs. Other studies on the vibrational properties of metal NWs have also been conducted by molecular dynamics (MD) simulations [8, 23, 24]. It is noticed that most of these studies have assumed a priori that NWs oscillate in a single plane. According to the work by Conley et al. [25], NW resonator can suddenly transit from a planar motion to whirling, 'jump rope' like motion, i.e., nonlinear or nonplanar vibration. Similar dual-mode resonance has also been observed in ZnO nanobelts [26] and GaN NWs [27], which is expected to open up a variety of new modalities for the NEMS that could operate in the nonlinear regime.

It is believed that NWs will vibrate in all planes with an identical frequency if the cross-section is symmetry. However, once this symmetry is broken, the single vibrational resonance peak will split into two closely spaced peaks of similar amplitude, with the peaks corresponding to vibrations in orthogonal planes [28]. Upon this fact, Gil-Santos et al. [28] proposed a new approach to mass sensing and stiffness spectroscopy, which allows the mass, stiffness and azimuthal arrival direction of the adsorbate to be determined. Our recent work [29] reported that the <110> FCC metal NWs (with circular or square cross-section) naturally possess two closely spaced resonance frequencies due to the specific lattice spacing in the {110} atomic layers, i.e., the NW exhibit a beat phenomenon or dual-mode vibration. Moreover, according to the recent experimental reports that the <110> NWs could be controlled to grow with a triangular cross-section [30], rhombic or even truncated rhombic cross-section [31]. It is noticed that, such asymmetric cross-section would leave the NW vibrating in two orthogonal planes, i.e., under dual-mode vibration. Thus, these NWs could be a good candidate for the application proposed by Gil-Santos et al. [28], which naturally exhibit two resonance frequencies.

However, it is found that the understanding of the dual-mode vibration of NWs with triangular, rhombic or truncated rhombic cross-section is still lack in the current literature, a few previous works can be found regarding the tensile and bending behaviors of such NWs by using MD simulation [32-34]. Because of this, it is crucial to study the mechanical properties of <110> metal NWs with these kinds of cross-sections as obtained through vibration, or resonance tests and simulations, which could benefit their applications as resonators. Thus, we perform such a comprehensive investigation using large scale MD simulations in the present work, and the surface effects on this dual-mode vibration is discussed based on the modified Euler-Bernoulli beam theory.

## 2. Numerical and Theoretical Basics

Large-scale MD simulations were carried out on <110> orientated Ag NWs with triangular, rhombic and truncated rhombic cross-sections. For different NWs, a constant aspect ratio of 10 is selected, with different cross-sectional size ranging from 3-8 nm. We modelled Ag using the embedded-atom-method (EAM) potential developed by Foiles et al. [35] This potential was fitted to a group of parameters, including cohesive energy, equilibrium lattice constant, bulk modulus, and others including a lattice constant $a$ which is chosen as 0.409 nm [36].

During each simulation, the NW was first created assuming bulk lattice positions, and then relaxed to a minimum energy state using the conjugate gradient algorithm, i.e. the length of the NW was allowed to decrease in response to the tensile surface stress. We then used the Nose-Hoover thermostat [37, 38] to equilibrate the NW at a constant temperature 10 K (NVT ensemble) for 400 picoseconds (psec) at a time step of 4 femtoseconds while holding the newly obtained length of the NW fixed. Finally, the NWs are actuated by applying a sinusoidal velocity excitation $v(z) = \lambda \sin(kz)$ along the *x* or *y*-axis, where $\lambda$ is the actuation amplitude, and *k* equals $\pi / L$. As illustrated in figure 1(a), the two ends of the NW are fixed in all three directions to mimic a doubly clamped beam. No periodic boundary conditions were utilized at any point during the simulation process.

We also emphasize that the NW is modeled using an energy-conserving (NVE) ensemble during the free vibration process following the velocity actuation, and that the applied velocity field increased the total potential energy by less than 0.1%, which ensures that the oscillations occur in the linear regime. The overall simulation methodology to study the oscillatory properties of the NWs is identical to that used previously for metal NWs [8, 22, 24]. All simulations were performed using the open-source LAMMPS code developed at Sandia National Laboratories [39] .

For the free vibration of thin beam, the governing equation is given as below, while including the surface effects [18, 19] (both surface tension and surface elasticity)

$$(EI)^* \frac{\partial^4 \upsilon}{\partial z^4} - p(z,t) = -\rho A \frac{\partial^2 \upsilon}{\partial z^2} \tag{1}$$

where $\upsilon(z,t)$ is the NW transverse displacement, $\rho$ is the density and $A$ is the cross-sectional area of the NW. $(EI)^*$ is the effective flexural rigidity, which incorporates the surface elasticity according to the composite beam theory [40, 41]. $p(z,t)$ is the distributed transverse force resulted from the surface stress, which can be approximated as $p(z,t) = H\partial^2 \upsilon / \partial z^2$ according to the generalized Young-Laplace equation [42]. $H$ is a constant depending on the residual surface tension and the cross-sectional shape, e.g., for the rectangular cross-section, $H = 2\tau w$, where $w$ is the width, and $\tau$ is the surface stress given as $\tau = \tau^0 + E_s \varepsilon_z$. $\tau^0$ is the surface stress along NW longitudinal direction, $E_s$ is the surface elastic modulus, and $\varepsilon_z$ is the longitudinal strain of the surface caused by the force acting on the NW. By assuming small deformation, $\tau = \tau^0$ . Note that, small deformation approximation will be adopted through the present work. For the doubly clamped end condition, the characteristic equation equals [18]

$$\lambda_1 \lambda_2 (\cos \lambda_1 L - \cosh \lambda_2 L)^2 + (\lambda_1 \sin \lambda_1 L + \lambda_2 \sinh \lambda_2 L)(\lambda_2 \sin \lambda_1 L - \lambda_1 \sinh \lambda_2 L) = 0 \tag{2}$$

Here,

$$\begin{cases} \lambda_1 = \sqrt{\sqrt{\left(\frac{\eta}{2L^2}\right)^2 + \left(\frac{\omega}{\kappa}\right)^2} - \frac{\eta}{2L^2}} \\ \lambda_2 = \sqrt{\sqrt{\left(\frac{\eta}{2L^2}\right)^2 + \left(\frac{\omega}{\kappa}\right)^2} + \frac{\eta}{2L^2}} \end{cases} \tag{3}$$

where $L$ is the NW length, $\kappa = \sqrt{(EI)^*/(\rho A)}$, $\omega$ is the angular resonance frequency, and $\eta$ is the nondimensional surface effect factor defined as $\eta = HL^2 / (EI)^*$.

## 3. Results and Discussion

Following discussions will focus on <110> Ag NWs with three kinds of cross-sectional geometries, i.e., rhombic, truncated rhombic and triangular cross-sections. Both the classical (continuum) and discrete models will be adopted to calculate the principal moments of inertia [29]. The discrete model is based on the discrete nature of the atomic system. In general, the moments of inertia are given as

$$\begin{cases} I_x = \int_A y^2 dA = \sum \left( y_n^2 A_n + I_a \right) \\ I_y = \int_A x^2 dA = \sum \left( x_n^2 A_n + I_a \right) \end{cases} \tag{4}$$

To discuss the surface effects, the normalized resonance frequency $R_f$ is defined as the ratio of the two first mode resonance frequencies along the two orthogonal vibrational planes (i.e., $f_x/f_y$). Several numerical testing will first be conducted to affirm that for the asymmetric cross-section, the NW will under a dual-mode vibration once the actuation direction differs from the two principal axes of inertia. Continue discussions will focus on how the surface effects influence the dual-mode vibration of the NW.

### 3.1. Dual-mode Vibration of Nanowires

Figure 2 illustrates the four types of cross-sections being studied. For each case, we consider three actuation directions as highlighted by the green and red arrows in figure 2 (i.e., *x*, *y* and *x'*-axes). Due to the similarity of the results, only the results from rhombic NWs are presented here, other results can be found in the Supplemental Materials.

Figure 3 shows the MD results for the NW with rhombic cross-section during the free vibration for a total of 7600 psec, the actuation is applied in the *x* or *x'*-axis. Generally, for the NW under the actuation along the *x*-axis, the external energy (*EE*) amplitude decreases as a linear function of time, where the *EE* is defined as the difference in the potential energy before and after the transverse velocity actuation is applied to the NW [8, 22]. As demonstrated in figure 3(a), no obvious *EE* dissipation is observed during the time of 0-2200 psec, which indicates a high quality (Q)-factor. Whereas, for the NW under the actuation along the *x'*-axis, *EE* amplitude appears highly nonlinear. Utilizing the fast Fourier transform (FFT) [43], two frequency components are identified in figure 3(d)

as 13.74 GHz and 19.13 GHz for the *EE* spectrum in figure 3(c). We note that the larger value is the same as identified from the *EE* spectrum in figure 3(a), and the smaller one is the same as obtained from the *EE* spectrum for the NW under the actuation along *y*-axis (see Supplemental Materials for details). This result indicates that the NW is under a dual-mode vibration that is comprised of two orthogonal vibrational components when the actuation direction is deviated from *x* or *y*-axis. Other MD simulations are then conducted for the NW with truncated rhombic and triangular cross-sections, from which the appearance of the dual-mode vibration is also observed. Therefore, considering the apparent generality of the dual-mode vibration for the <110> NW (with rhombic, truncated rhombic or triangular cross-section), we then proceed to study the surface effects on this phenomenon. To mention that all following MD simulations are carried out for a group of Ag NWs with the aspect ratio of 10, and the actuation direction of *x'*-axis (see figure 2(a)).

### 3.2. Nanowire with Rhombic Cross-section

The rhombic cross-section is firstly discussed. As illustrated in figure 4, the rhombic cross-section of a <110> Ag NW is enclosed by four {111} surfaces. For the continuum model, the principal moments of inertia are given as

$$\begin{cases} I_{cx} = b^4 \sin^3\phi\cos\phi/3 \\ I_{cy} = b^4 \sin\phi\cos^3\phi/3 \end{cases}, \tag{5a}$$

and the area equals $A = 2b^2\sin\phi\cos\phi$. Here, $b$ is the side length, and $\phi$ is the angle as specified in figure 4. On the other hand, under the discrete model, we have

$$\begin{cases} I_{dx} = (2N+1)I_a + \sum_{i=1}^{N}\left[2(N-i)+1\right]\left[A_a a^2 i^2 + 2I_a\right] \\ I_{dy} = (2N+1)I_a + 2\sum_{i=1}^{N}\left[2(N-i)+1\right]\left[A_a a^2 i^2 + I_a\right] \end{cases}, \tag{5b}$$

and the area equals $A = (2N^2+2N+1)A_a$, where $N$ is an integer and related with the side length $b$ by $b = Na/\cos\phi$. $a$ is the lattice constant, $A_a$ is the projection area of a single atom and $I_a$ is the principal moment of inertia around the atom's own axis.

To evaluate the surface effects, the NWs are modeled as a superposition of surface layers and bulk volume follow previous researchers [40, 44]. The grey areas in figure 4 schematically represent the {111} surface layers with an elastic modulus $E_1$ and thickness $t_1$. The thickness $t_1$ is assumed to be much smaller comparing with the cross-section size $b$. The relation between $E_1$ and $E_{s1}$ is $E_{s1} = E_1 t_1$ [19]. According to the composite beam theory with the assumptions of $t_1 \ll b$, the effective flexural rigidity is approximated as

$$\begin{cases} (EI)_x^* = EI_x + 4E_1\int_0^{b\sin\phi} y^2 t_1 / \sin\phi dy = EI_x + 4E_{s1}b^3\sin^2\phi/3 \\ (EI)_y^* = EI_y + 4E_1\int_0^{b\cos\phi} x^2 t_1 / \cos\phi dx = EI_y + 4E_{s1}b^3\cos^2\phi/3 \end{cases}, \quad (5c)$$

where $E_{s1}$ is the elastic modulus of the {111} surface. In the meanwhile, from the Young-Laplace equation, the distributed transverse force $p(x,t)$ can be approximated as

$$\begin{cases} p(z,t)_x = 4\tau_1 b\sin\phi\dfrac{\delta^2\upsilon}{\delta z^2} \\ p(z,t)_y = 4\tau_1 b\cos\phi\dfrac{\delta^2\upsilon}{\delta z^2} \end{cases}, \quad (5d)$$

where $\tau_1$ is the {111} surface stress along the NW longitudinal direction. For the Ag NW, $E_{s1}$ equals -1.39 N/m, $\tau_1$ equals 0.65 N/m and $E$ equals 76 GPa [45, 40].

Recall Eqs. (2) and (3), we now compare the first mode natural frequencies of Ag NW between the predictions by the classical Euler-Bernoulli beam theory, modified Euler-Bernoulli beam theory with surface effects and MD simulations. As revealed in figure 5(a), for both two natural frequencies ( $f_x$ and $f_y$ ), the discrete model enhanced the theoretical predictions comparing with the MD results. It is evident that, the inclusion of the surface effects increases the first natural frequencies for both discrete and continuum models, which also exhibit better agreements with MD results. Furthermore, it is noticed that, the theoretical predictions become closer to MD results for NWs with larger cross-section (especially for the frequency of $f_y$ ), which claims the crucial influence from surface effects on ultrathin NWs.

Figure 5(b) reveals the surface effects on the dual-mode vibration of the NWs. As is seen, for the classical beam model, the normalized resonance frequency $R_f$ is a constant value, which equals $\sqrt{2}$ , while utilizing the discrete model, $R_f$ appears almost unchanged with minor decrease for ultra small cross-sections. However, the consideration of the surface contribution obviously decreased the gap between the two first natural frequencies, i.e., $R_f$ shows considerable decrease comparing with the classical beam model. Particularly, this trend is found to agree with the MD results. Just as expected, with the increase of the cross-sectional size, the influence of the surface effects diminishes, and the normalized resonance frequency converges to the classical value of $\sqrt{2}$ .

### 3.3. Nanowire with Triangular Cross-section (α)

As reported by previous researchers, <110> NWs can be controlled to grow with two kinds of triangular cross-sections during the synthesization process [30]. One of them is illustrated in figure 6 (denoted as triangle α), which is enclosed by two {111} surfaces and one {110} surface. For the continuum model, the principal moments of inertia around its centroid are given as

$$\begin{cases} I_{cx} = b^4 \sin^3\phi\cos\phi / 18 \\ I_{cy} = b^4 \sin\phi\cos^3\phi / 6 \end{cases}, \tag{6a}$$

and the area equals $A = b^2 \sin\phi\cos\phi$. To aware that for the discrete model, the centroid position offsets from $h/3$ to $h(2N+1)/[6(N+1)]$, where $N$ is an integer and related with the side length $b$ by $b = Na/\cos\phi$. $h$ is the height of the triangle (see figure 6) and equals $h = b\sin\phi$. Therefore, the principal moments of inertia are induced as

$$\begin{cases} I_{dx} = \sum_{i=1}^{N}\left[2N-2i+3\right]\left\{A_a\left[(i-1)a\sqrt{2}/2 - h(2N+1)/6(N+1)\right]^2 + I_a\right\} \\ I_{dy} = (N+1)I_a + 2\sum_{i=1}^{N}\left[(N-i)+1\right]\left[A_a a^2 i^2 + I_a\right] \end{cases}, \tag{6b}$$

and the area equals $A = (N^2+2N+1)A_a$.

Following previous surface layers assumption, i.e., consider the {111} and {110} surface layers with an identical thickness $t_1$, and an elastic modulus $E_1$ and $E_2$, respectively. The relation between $E_2$ and $E_{s2}$ is $E_{s2} = E_2 t_1$. According to the composite beam theory, the effective flexural rigidity for the continuum model can be approximated as

$$\begin{cases} (EI)_x^* = EI_x + E_2(2bt_1\cos\phi)(b\sin\phi/3)^2 + 2E_1\int_{-b\sin\phi/3}^{2b\sin\phi/3} y^2 t_1/\sin\phi dy \\ (EI)_y^* = EI_y + E_2\int_{-b\cos\phi}^{b\cos\phi} x^2 t dA + 2E_1\int_0^{b\cos\phi} x^2 t_1/\cos\phi dx \end{cases}, \text{ that is}$$

$$\begin{cases} (EI)_x^* = EI_x + 2E_{s2}b^3\sin^2\phi\cos\phi/9 + 2E_{s1}b^3\sin^2\phi/9 \\ (EI)_y^* = EI_y + 2E_{s2}b^3\cos^3\phi/3 + 2E_{s1}b^3\cos^2\phi/3 \end{cases}, \tag{6c}$$

where $E_{s2}$ is the elastic modulus of the {110} surface. Based on the Young-Laplace equation, the distributed transverse force $p(x,t)$ can be approximated as

$$\begin{cases} p(z,t)_x = 2\tau_1 b\sin\phi\dfrac{\delta^2\upsilon}{\delta z^2} \\ p(z,t)_y = (2\tau_1 b\cos\phi + 2\tau_2 b\cos\phi)\dfrac{\delta^2\upsilon}{\delta z^2} \end{cases} \tag{6d}$$

where $\tau_2$ is the {110} surface stress along the NW longitudinal direction. For the Ag NW, $E_{s2}$ equals -4.74N/m, $\tau_2$ equals 0.70 N/m [45].

Recall Eqs. (2) and (3), the first mode natural frequencies of Ag NW with triangular cross-section ($\alpha$) are compared between the predictions by different beam models and MD simulations. As shown in figure 7(a), for the first mode natural frequency along *x*-axis ($f_x$), the theoretical predictions are smaller than MD results. While, for $f_y$, the theoretical predictions with surface influence are overestimated. Similar as the results for the rhombic cross-section in figure 5(a), the predictions

appear closer to the MD results with the increase of the cross-sectional size, and the discrete model gives better estimation to the resonance frequency than the continuum model.

Figure 7(b) reveals the surface effects on the dual-mode vibration of the NWs. For the classical beam model, the normalized resonance frequency $R_f$ equals $\sqrt{6}$, which shows minor decrease under the discrete model. In the opposite, the inclusion of surface effects exerts an evident decrease to $R_f$. As seen in figure 7(b), the MD results demonstrate the same trend, and the influence from surface effects reduces as the cross-sectional size increases.

### 3.4. Nanowire with Triangular Cross-section (β)

Another kind of triangular cross-section is revealed in figure 8 (denoted as triangle $\beta$), which is enclosed by two {111} surfaces and one {100} surface. Similarly, for the continuum model, the principal moments of inertia are given as:

$$\begin{cases} I_{cx} = b^4 \sin^3\varphi\cos\varphi/18 \\ I_{cy} = b^4 \sin\varphi\cos^3\varphi/6 \end{cases}, \tag{7a}$$

and the area equals $A = b^2\sin\varphi\cos\varphi$. Here, $\varphi$ is the angle as specified in figure 8. For the discrete model, the principal moments of inertia are deduced as:

$$\begin{cases} I_{dx} = \left[2N-2i+3\right]\left\{A_a\left[(i-1)a - h(2N+1)/6(N+1)\right]^2 + I_a\right\} \\ I_{dy} = (N+1)I_a + \sum_{i=1}^{N}\left[(N-i)+1\right]\left[A_a a^2 i^2 + 2I_a\right] \end{cases}, \tag{7b}$$

and the area equals $A = (N^2+2N+1)A_a$, where $N$ is an integer and related with the side length $b$ by $b = Na/\sin\varphi$. $h$ is the height (see figure 8) and equals $h = Na$.

Consider the {100} surface layer with an elastic modulus $E_3$, thickness $t_1$ and the relation between $E_3$ and $E_{s3}$ is $E_{s3} = E_3 t_1$. Then, the effective flexural rigidity can be approximated as

$$\begin{cases} (EI)_x^* = EI_x + E_3(2bt_1\cos\varphi)(b\sin\varphi/3)^2 + 2E_1\int_{-b\sin\varphi/3}^{2b\sin\varphi/3} y^2 t_1/\sin\varphi dy \\ (EI)_y^* = EI_y + E_3\int_{-b\cos\varphi}^{b\cos\varphi} x^2 t_1 dA + 2E_1\int_0^{b\cos\varphi} x^2 t_1/\cos\varphi dx \end{cases}, \text{ that is}$$

$$\begin{cases} (EI)_x^* = EI_x + 2E_{s3}b^3\sin^2\varphi\cos\varphi/9 + 2E_{s1}b^3\sin^2\varphi/9 \\ (EI)_y^* = EI_y + 2E_{s3}b^3\cos^3\varphi/3 + 2E_{s1}b^3\cos^2\varphi/3 \end{cases} \tag{7c}$$

where $E_{s3} = E_3 t_1$, which is the elastic modulus of the {100} surface. From the Young-Laplace equation, the distributed transverse force $p(x,t)$ can be approximated as.

$$\begin{cases} p(z,t)_x = 2\tau_1 b \sin\varphi \dfrac{\delta^2 \upsilon}{\delta z^2} \\ p(z,t)_y = (2\tau_1 b\cos\varphi + 2\tau_3 b\cos\varphi)\dfrac{\delta^2 \upsilon}{\delta z^2} \end{cases} \tag{7d}$$

where $\tau_3$ is the {110} surface stress along the NW longitudinal direction. For the Ag NW, $E_{s3}$ equals 1.22 N/m, $\tau_3$ equals 0.89 N/m [45, 40].

According to Eqs. (2) and (3), the first mode natural frequencies of Ag NW with triangular cross-section ($\beta$) are compared between the predictions by different beam models and MD simulations. From figure 9(a), for the first mode natural frequency along *x*-axis ($f_x$), the continuum model with surface effects shows good agreements with MD results for cross-sectional size smaller than 6 nm. With the increase of cross-sectional size, the MD results become closer to the predictions by discrete model with surface effects. For the first mode natural frequency along *y*-axis ($f_y$), the continuum model with surface influence also provides better estimations than other models.

Figure 9(b) presents the surface effects on the dual-mode vibration of the NWs. Firstly, for the classical beam model, the normalized resonance frequency $R_f$ equals $\sqrt{6}/2$, which shows minor decrease for ultra small cross-sections under the discrete model. Similar as previous cases, the inclusion of surface influence also leads to an apparent decrease to the normalized resonance frequency $R_f$, which is consistent with the MD results. It is expected that, with the increase of the cross-sectional size, the influence of the surface effects diminishes, and normalized resonance frequency converges to the classical value of $\sqrt{6}/2$.

### 3.5. Nanowire with Truncated Rhombic Cross-section

Recently, Kolibal et al. [31] reported that the <110> orientated Ge NWs can be controlled to grow with a truncated rhombic cross-section as shown in figure 10, which is enclosed by four {111} surfaces and two {100} surface. To investigate such specific cross-sectional geometry, we consider the rhombic cross-section being truncated at the middle of its side as illustrated in figure 10. For the continuum model, the principal moments of inertia are given as

$$\begin{cases} I_x = 5b^4 \sin^3\phi\cos\phi/16 \\ I_y = 5b^4 \sin\phi\cos^3\phi/48 \end{cases}, \tag{8a}$$

and the area equals $A = 3b^2 \sin\varphi\cos\varphi/2$. Under the discrete model, the principal moments of inertia are deduced as

$$\begin{cases} I_x = (N+1)I_a + (N+1)\sum_{i=1}^{N/2}(A_a a^2 i^2 + 2I_a) + \sum_{j=N/2+1}^{N}\left[2(N-j)+1\right]\left[A_a a^2 j^2 + 2I_a\right] \\ I_y = (2N+1)I_a + 2\sum_{i=1}^{N/2}\left[2(N-i)+1\right]\left[A_a a^2 i^2 + I_a\right] \end{cases}, \tag{8b}$$

and the area equals $A = (3N^2/2 + 2N + 1)A_a$, where $N$ is an even integer and related with the side length $b$ by $b = Na/(2\cos\phi)$.

Under the conception of surface layers and follow the assumptions made to the {100} and {111} surface layers, the effective flexural rigidity is approximated as below

$$\begin{cases} (EI)_x^* = EI_x + 2E_3\int_{-b\sin\phi/2}^{b\sin\phi/2} y^2 t_1 dy + 4E_1\int_{b\sin\phi/2}^{b\sin\phi} y^2 t_1/\sin\phi dy \\ (EI)_y^* = EI_y + 2E_3(b\sin\phi t_1)(b\cos\phi/2)^2 + 4E_1\int_0^{b\cos\phi/2} x^2 t_1/\cos\phi dx \end{cases}, \text{ that is}$$

$$\begin{cases} (EI)_x^* = EI_x + E_{s3}b^3\sin^3\phi/6 + 7E_{s1}b^3\sin^2\phi/6 \\ (EI)_y^* = EI_y + E_{s3}b^3\sin\phi\cos^2\phi/2 + E_{s1}b^3\cos^2\phi/6 \end{cases} \tag{8c}$$

From the Young-Laplace equation, the distributed transverse force $p(x,t)$ can be approximated as

$$\begin{cases} p(z,t)_x = (2\tau_1 b\sin\varphi + 2\tau_3 b\sin\varphi)\dfrac{\delta^2\upsilon}{\delta z^2} \\ p(z,t)_y = 2\tau_1 b\cos\varphi\dfrac{\delta^2\upsilon}{\delta z^2} \end{cases} \tag{8d}$$

Refer Eqs. (2) and (3), the first mode natural frequencies of Ag NW with truncated rhombic cross-section are compared between the predictions by different beam models and MD simulations. As revealed in figure 11(a), the first mode natural frequency $f_y$ from MD simulations exhibit good agreement with the predictions by the discrete model with surface effect. In the other hand, the first mode natural frequency $f_x$ from MD results appear good agreement with the predictions by the continuum model with surface effect when the cross-section size is smaller than 6 nm, which becomes closer to the predictions by the discrete model with surface effects with a increase of the cross-sectional size.

Figure 11(b) reveals the surface effects on the dual-mode vibration of the NWs with truncated rhombic cross-section. Basically, for the classical beam model, the normalized resonance frequency $R_f$ equals $\sqrt{6}/3$, whist utilizing the discrete model, a relative obvious increase appeared for ultra small cross-sections. The consideration of the surface contribution apparently decreased the gap between the two first natural frequencies, which leads certain increase to the $R_f$. Particularly, this trend is found to agree with the MD results. It is appeared that, with the increase of the cross-sectional size, the influence of the surface effects diminishes, and normalized resonance frequency converges to the classical value of $\sqrt{6}/3$.

### 3.6 Discussions

Generally, according to the above results, the modified beam models with surface effects show better estimations of the first natural frequency for different cross-sectional geometries than the classical beam model. However, these models still show certain inaccuracy, which might arise from the simplified or inaccurate interpretation of the surface effects. As is reported for ultrathin NWs [46], the contribution of surface-stress-induced surface elasticity to the NW's behaviors is always considerably smaller than that due to the nonlinear elasticity of the NW core. Recent work also reported that for NWs under bending [47], the current inclusion of the surface effect into the Euler-Bernoulli beam model still suffers from certain overestimating (especially for ultrathin NWs), and by introducing an inverse NW core effect (i.e., reduce the surface effect with a factor that smaller than one), the theoretical predictions appears considerable improvement. It is interesting to mention that, such scenario is also observed in figures 5, 7, 9 and 11, from which, the modified beam models exhibit closer predictions to MD results for the rhombic cross-section than other three cross-sections (i.e., both triangular and truncated cross-sections), since either triangular or truncated rhombic cross-section area is much smaller (means thinner) than that of the rhombic cross-section for the identical side length $b$, therefore, the theoretical predictions appear poorer.

Conclusively, to depict the occurrence of dual-mode vibration, the normalized resonance frequency $R_f$ can be generalized and re-defined as an overall asymmetric factor $\xi$ as

$$\xi = f_x / f_y = \xi_{cg} + \xi_{ls}(b) + \xi_{se}(b) \tag{9}$$

$\xi_{cg}$ represents the asymmetric factor from the cross-sectional geometry, which equals $\sqrt{I_y / I_x}$. $\xi_{ls}$ and $\xi_{se}$ represent the asymmetric factor from the different lattice spacing and surface effect, respectively. Both of them are a function of the cross-sectional size *b*. According to Eq. (9), the overall asymmetric factor ($\xi$ or $R_f$) for the four theoretical models discussed in this paper is actually a sum from different asymmetric factors, i.e., for the continuum model, $\xi_C = \xi_{cg}$; for the continuum-surface model, $\xi_{CS} = \xi_{cg} + \xi_{se}(b)$; for the discrete model, $\xi_D = \xi_{cg} + \xi_{ls}(b)$; for the discrete-surface model, $\xi_{DS} = \xi_{cg} + \xi_{ls}(b) + \xi_{se}(b)$. Based on these models, it is easy to find that $\xi_{ls} = \xi_D - \xi_C$. Aware that, due to the difference of the cross-sectional area, the asymmetric factor $\xi_{se}$ in the discrete-surface model is cross influenced by $\xi_{ls}$. To avoid such influence, $\xi_{se}$ can be calculated from $\xi_{se} = \xi_{CS} - \xi_C$.

According to the results in figures 5(b), 7(b), 9(b) and 11(b), $\xi_{ls}$ exerts minor influence to $\xi_{cg}$, especially for the rhombic, and triangular cross-sections. Whereas, the inclusion of surface effect (i.e., $\xi_{se}$) shows a considerably obvious influence to the overall asymmetric factor. These results indicate that for the symmetrical cross-section geometry such as square or circular (when $\xi_{cg} = 1$), $\xi_{ls}$ and $\xi_{se}$

will induce remarkable influence to the resonance behaviours of NWs, i.e., $\xi_{ls}$ and $\xi_{se}$ will raise the deviation of $\xi$ from one and the difference between the two first natural frequencies, which will attract a beat phenomenon as reported by Zhan et al. [29]. While for the asymmetrical cross-section geometry (e.g., rhombic, triangular or truncated rhombic), $\xi_{ls}$ and $\xi_{se}$ usually intend to mitigate the dual-mode vibration, i.e., reduce the deviation of $\xi$ from one and the difference between the two first natural frequencies. However, since $\xi_{cg}$ is a constant value that already apparently different from one for the asymmetrical cross-section, hence, the influence from $\xi_{ls}$ or $\xi_{se}$ will be greatly concealed or hided, and an apparent dual-mode vibration still arises. It is no doubt that, larger deviation of $\xi$ from one means more significant difference between the two first mode natural frequencies, and induces more apparent dual-mode vibration.

## 4. Conclusion

Based on the large-scale MD simulations and Euler-Bernoulli beam models including and ignoring surface effects, we study the dual-mode vibration of doubly clamped <110> orientated Ag NWs with three kinds of cross-sections, i.e., rhombic, truncated rhombic, and triangular cross-sections. The surface effects on the dual-mode vibration of NWs are studied by incorporating the generalized Young-Laplace equation into Euler-Bernoulli beam theory. Due to the different lattice spacing in principal axes of inertia of the {110} atomic layers, the NW is also modeled as a discrete system to reveal the influence from such specific atomic arrangement. Major conclusions are summarized as below:

1) The <110> Ag NW with rhombic, truncated rhombic or triangular cross-section will under a dual-mode vibration if the actuation direction is deviated from the two principal axes of inertia;

2) For the four types of cross-section geometries, the classical beam model shows underestimated predictions for the two first natural frequencies comparing with the MD results, whist the discrete model is found to enhance the predictions by the continuum model;

3) The predictions by the beam theory with the incorporation of surface effects uniformly larger than the classical beam model, which is agreed with previous researchers that a positive surface stress increases the resonance frequencies of doubly clamped NWs.

4) It is found that though the modified beam model (with surface effects) provides better estimations to the resonance frequency than the classical beam model, the values still appear certain gap comparing with the MD results, especially for the two kinds of triangular cross-sections. Particularly, we note that, the theoretical predictions exhibit better agreement with MD results for larger cross-sectional size. Hence, it is concluded that for ultrathin NWs, current consideration of surface effects is still experiencing certain inaccuracy, and the consideration of the nonlinear elasticity of the NW core might be able to overcome such deficiency.

5) For all different cross-sections, the inclusion of surface effects is found to reduce the difference between the two first mode natural frequencies. This trend is observed consistent with MD results.

In summary, this study provides a first comprehensive investigation on the dual-mode vibration of <110> oriented Ag NWs with rhombic, truncated rhombic and triangular cross-sections. The influence of surface effects on the dual-mode vibration is extensively discussed. This study is supposed to benefit the applications of NWs that acting as a resonating beam.

**Acknowledgement**

The authors heartily appreciate Professor Harold S. Park at Boston University for his insightful suggestions in preparing this paper. In addition, this work is supported by the ARC Future Fellowship grant (FT100100172).

## References

[1] Craighead H G 2000 Nanoelectromechanical systems *Science* **290** 1532-5
[2] Husain A, Hone J, Postma H W C, Huang X, Drake T, Barbic M, Scherer A and Roukes M 2003 Nanowire-based very-high-frequency electromechanical resonator *Appl. Phys. Lett.* **83** 1240
[3] Ma R M, Dai L, Huo H B, Xu W J and Qin G 2007 High-performance logic circuits constructed on single CdS nanowires *Nano Lett.* **7** 3300-4
[4] Liao M, Hishita S, Watanabe E, Koizumi S and Koide Y 2010 Suspended Single‐Crystal Diamond Nanowires for High‐Performance Nanoelectromechanical Switches *Adv. Mater.* **22** 5393-7
[5] Wang Z L and Song J 2006 Piezoelectric nanogenerators based on zinc oxide nanowire arrays *Science* **312** 242
[6] Xie P, Xiong Q, Fang Y, Qing Q and Lieber C M 2011 Local electrical potential detection of DNA by nanowire-nanopore sensors *Nat. Nanotechnol.* **7** 119-25
[7] Eom K, Park H S, Yoon D S and Kwon T 2011 Nanomechanical resonators and their applications in biological/chemical detection: Nanomechanics principles *Phys. Rep.* **503** 115-63
[8] Kim S Y and Park H S 2008 Utilizing mechanical strain to mitigate the intrinsic loss mechanisms in oscillating metal nanowires *Phys. Rev. Lett.* **101** 215502
[9] Li M, Tang H and Roukes M 2007 Ultra-sensitive NEMS-based cantilevers for sensing, scanned probe and very high-frequency applications *Nat. Nanotechnol.* **2** 114-20
[10] Carr D W, Evoy S, Sekaric L, Craighead H and Parpia J 1999 Measurement of mechanical resonance and losses in nanometer scale silicon wires *Appl. Phys. Lett.* **75** 920-2
[11] Sekaric L, Parpia J, Craighead H, Feygelson T, Houston B and Butler J 2002 Nanomechanical resonant structures in nanocrystalline diamond *Appl. Phys. Lett.* **81** 4455
[12] Verbridge S S, Parpia J M, Reichenbach R B, Bellan L M and Craighead H 2006 High quality factor resonance at room temperature with nanostrings under high tensile stress *J. Appl. Phys.* **99** 124304
[13] Yang Y, Ekinci K, Huang X, Schiavone L, Roukes M, Zorman C and Mehregany M 2001 Monocrystalline silicon carbide nanoelectromechanical systems *Appl. Phys. Lett.* **78** 162
[14] Feng X, He R, Yang P and Roukes M 2007 Very high frequency silicon nanowire electromechanical resonators *Nano Lett.* **7** 1953-9
[15] Yang Y, Callegari C, Feng X and Roukes M 2011 Surface Adsorbate Fluctuations and Noise in Nanoelectromechanical Systems *Nano Lett.* **11** 1753-9
[16] Chen C Q, Shi Y, Zhang Y S, Zhu J and Yan Y J 2006 Size dependence of Young's modulus in ZnO nanowires *Phys. Rev. Lett.* **96** 075505
[17] Park H S, Cai W, Espinosa H D and Huang H 2009 Mechanics of crystalline nanowires *MRS Bull.* **34** 178-83
[18] He J and Lilley C 2008 Surface stress effect on bending resonance of nanowires with different boundary conditions *Appl. Phys. Lett.* **93** 263108
[19] Wang G F and Feng X Q 2007 Effects of surface elasticity and residual surface tension on the natural frequency of microbeams *Appl. Phys. Lett.* **90** 231904
[20] Park H S and Klein P A 2008 Surface stress effects on the resonant properties of metal nanowires: the importance of finite deformation kinematics and the impact of the residual surface stress *J. Mech. Phys. Solids* **56** 3144-66
[21] Park H S 2008 Surface stress effects on the resonant properties of silicon nanowires *J. Appl. Phys.* **103** 123504
[22] Kim S Y and Park H S 2009 The importance of edge effects on the intrinsic loss mechanisms of graphene nanoresonators *Nano Lett.* **9** 969-74

[23] Olsson P A T, Park H S and Lidström P C 2010 The Influence of shearing and rotary inertia on the resonant properties of gold nanowires *J. Appl. Phys.* **108** 104312
[24] Zhan H F and Gu Y T 2012 A fundamental numerical and theoretical study for the vibrational properties of nanowires *J. Appl. Phys.* **111** 124303-9
[25] Conley W G, Raman A, Krousgrill C M and Mohammadi S 2008 Nonlinear and nonplanar dynamics of suspended nanotube and nanowire resonators *Nano Lett.* **8** 1590-5
[26] Bai X, Gao P, Wang Z L and Wang E 2003 Dual-mode mechanical resonance of individual ZnO nanobelts *Appl. Phys. Lett.* **82** 4806
[27] Nam C Y, Jaroenapibal P, Tham D, Luzzi D E, Evoy S and Fischer J E 2006 Diameter-dependent electromechanical properties of GaN nanowires *Nano Lett.* **6** 153-8
[28] Gil-Santos E, Ramos D, Martínez J, Fernández-Regúlez M, García R, San Paulo Á, Calleja M and Tamayo J 2010 Nanomechanical mass sensing and stiffness spectrometry based on two-dimensional vibrations of resonant nanowires *Nat. Nanotechnol.* **5** 641-5
[29] Zhan H, Gu Y and Park H S 2012 Beat Phenomena in Metal Nanowires, and their Implications for Resonance-Based Elastic Property Measurements *Nanoscale* **10.1039/C2NR31545A**
[30] Yoo Y, Yoon I, Lee H, Ahn J, Ahn J P and Kim B 2010 Pattern-Selective Epitaxial Growth of Twin-Free Pd Nanowires from Supported Nanocrystal Seeds *ACS Nano* **4** 2919-27
[31] Kolíbal M, Kalousek R, Vystavěl T, Novák L and Šikola T 2012 Controlled faceting in< 110> germanium nanowire growth by switching between vapor-liquid-solid and vapor-solid-solid growth *Appl. Phys. Lett.* **100** 203102--4
[32] Park H, Gall K and Zimmerman J 2006 Deformation of FCC nanowires by twinning and slip *J. Mech. Phys. Solids* **54** 1862-81
[33] Leach A M, McDowell M and Gall K 2007 Deformation of Top Down and Bottom Up Silver Nanowires *Adv. Funct. Mater.* **17** 43-53
[34] McDowell M, Leach A and Gall K 2008 Bending and tensile deformation of metallic nanowires *Modell. Simul. Mater. Sci. Eng.* **16** 045003
[35] Foiles S M, Baskes M I and Daw M S 1986 Embedded-atom-method functions for the fcc metals Cu, Ag, Au, Ni, Pd, Pt, and their alloys *Phys. Rev. B* **33** 7983-91
[36] Voter A 1993 Embedded atom method potentials for seven fcc metals: Ni, Pd, Pt, Cu, Ag, Au, and Al *Los Alamos Unclassified Technical Report LA-UR* 93-3901
[37] Hoover W G 1985 Canonical dynamics: Equilibrium phase-space distributions *Phys. Rev. A* **31** 1695-7
[38] Nosé S 1984 A unified formulation of the constant temperature molecular dynamics methods *J. Chem. Phys.* **81** 511
[39] Plimpton S 1995 Fast parallel algorithms for short-range molecular dynamics *J. Comput. Phys.* **117** 1-19
[40] He J and Lilley C M 2008 Surface effect on the elastic behavior of static bending nanowires *Nano Lett.* **8** 1798-802
[41] Wang G and Feng X 2009 Surface effects on buckling of nanowires under uniaxial compression *Appl. Phys. Lett.* **94** 141913
[42] Chen T, Chiu M S and Weng C N 2006 Derivation of the generalized Young-Laplace equation of curved interfaces in nanoscaled solids *J. Appl. Phys.* **100** 074308
[43] Brigham E O and Morrow R 1967 The fast Fourier transform *Spectrum, IEEE* **4** 63-70
[44] Jing G Y, Duan H L, Sun X M, Zhang Z S, Xu J, Li Y D, Wang J X and Yu D P 2006 Surface effects on elastic properties of silver nanowires: Contact atomic-force microscopy *Phys. Rev. B* **73** 235409
[45] Shenoy V B 2005 Atomistic calculations of elastic properties of metallic fcc crystal surfaces *Phys. Rev. B* **71** 094104
[46] Liang H, Upmanyu M and Huang H 2005 Size-dependent elasticity of nanowires: Nonlinear effects *Phys. Rev. B* **71** 241403
[47] Zhan H F and Gu Y T 2012 Modified beam theories for bending properties of nanowires considering surface/intrinsic effects and axial extension effect *J. Appl. Phys.* **111** 084305

# Table of figures

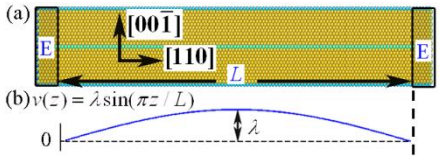


**FIG.1** (a) A doubly clamped Ag NW model for the vibration tests with a rhombic cross-section. 'E' represents the fixed end. $x$, $y$ and $z$-axes represent the directions of $[00\bar{1}]$, $[\bar{1}10]$ and $[110]$, respectively. (b) The profile of a sinusoidal velocity actuation.

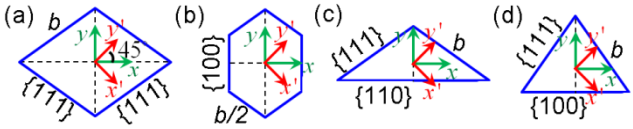


**FIG.2** Schematics of different cross-sectional geometries. (a) Rhombic cross-section. (b) Truncated rhombic cross-section. (c) Triangular cross-section $\alpha$. (d) Triangular cross-section $\beta$. $x$, $y$ and $x'$ refer three different actuation directions that originated at the centroid. $b$ represents the cross-sectional size. For (a), (b) and (c), $x$ and $y$-axes represent the direction of $[00\bar{1}]$ and $[\bar{1}10]$, respectively. For (d), $x$ and $y$-axes represent the direction of $[1\bar{1}0]$ and $[00\bar{1}]$, respectively.

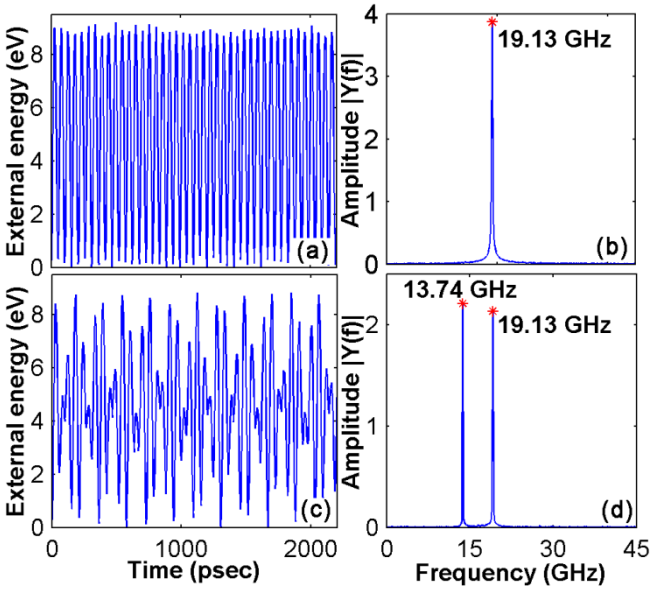


**FIG.3** MD results for the <110> Ag NW with a rhombic cross-section and a side length of 3 nm. (a) Time history of the external energy for a free vibration simulation at 10 K (time is truncated at 2200 psec). Actuation is exerted along $x$-axis. (b) The corresponding frequency spectrum of the external energy using FFT analysis (truncated at a frequency of 45 GHz). (c) Time history of the external energy for a free vibration simulation at 10 K (time is truncated at 2200 psec). Actuation is exerted along $x'$-axis. (d) The corresponding frequency spectrum of the external energy using FFT analysis (truncated at a frequency of 45 GHz).

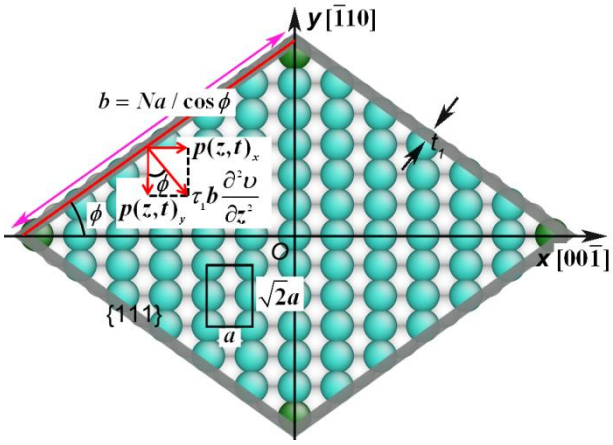


**FIG.4** Atomic layer of the rhombic cross-section, the grey edge schematically refers the surface layers.

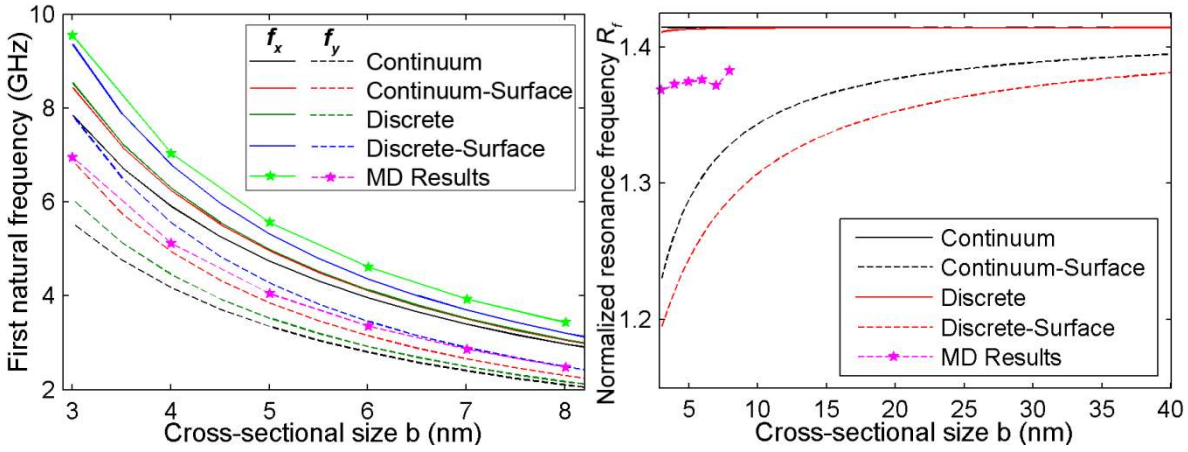


**FIG. 5** (a) Comparison of the first natural frequencies between theoretical predictions and MD results. (b) Comparison of the normalized resonance frequency ( $R_f = f_x / f_y$ ) between theoretical predictions and MD results.

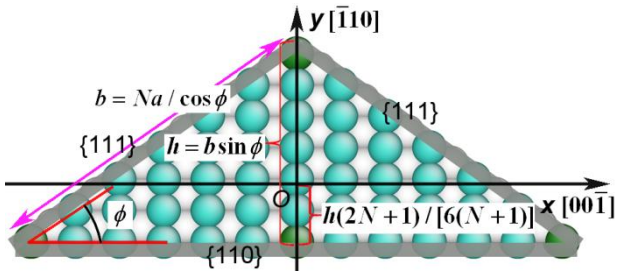


**FIG.6** Atomic layer of the triangular cross-section ( $\alpha$ ), the grey edge schematically refers the surface layers.

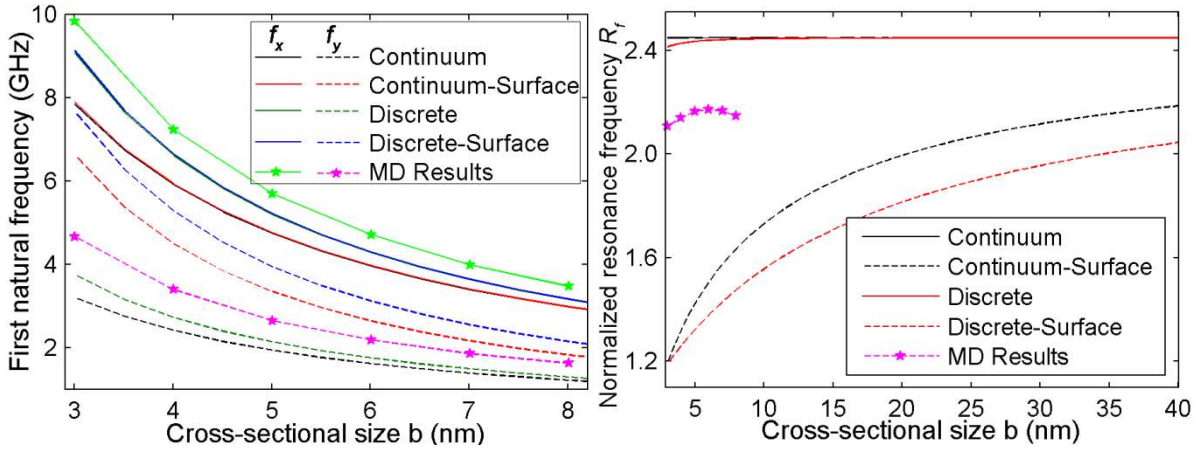


**FIG.7** (a) Comparison of the first natural frequencies between theoretical predictions and MD results. (b) Comparison of the normalized resonance frequency ( $R_f = f_x / f_y$ ) between theoretical predictions and MD results.

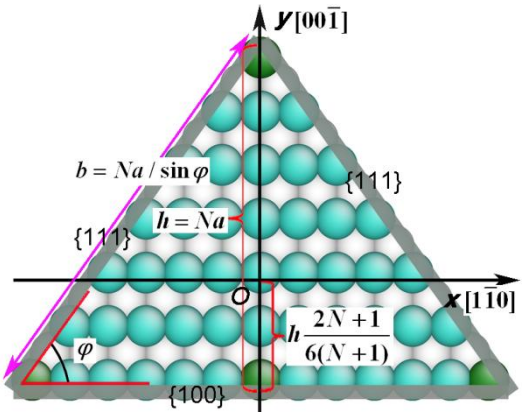


**FIG.8** Atomic arrangement of the triangular cross-section ( $\beta$ ), the grey edge schematically refers the surface layers.

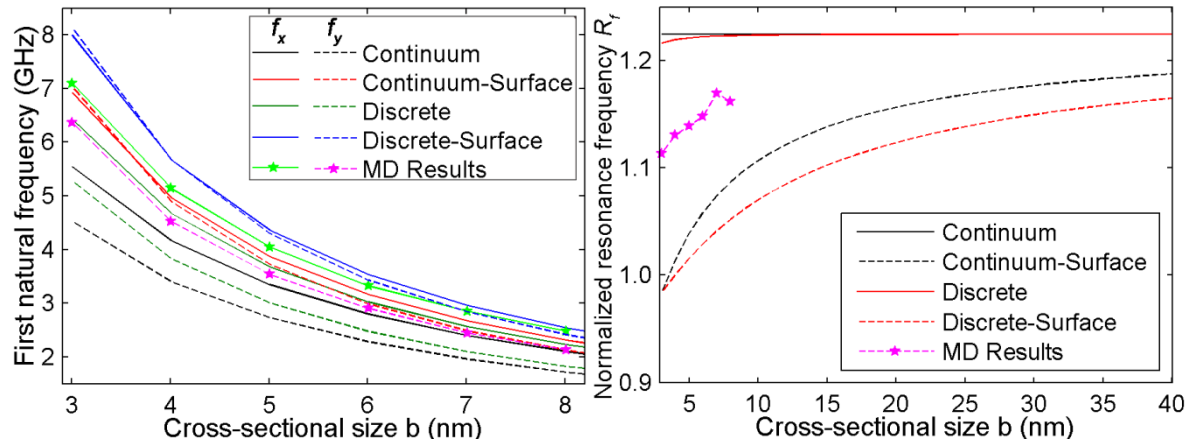


**FIG.9** (a) Comparison of the first natural frequencies between theoretical predictions and MD results. (b) Comparison of the normalized resonance frequency ( $R_f = f_x / f_y$ ) between theoretical predictions and MD results.

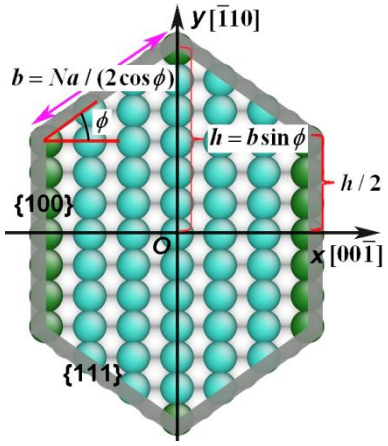


**FIG.10.** Atomic arrangement of the truncated rhombic cross-section, the grey edge schematically refers the surface layers.

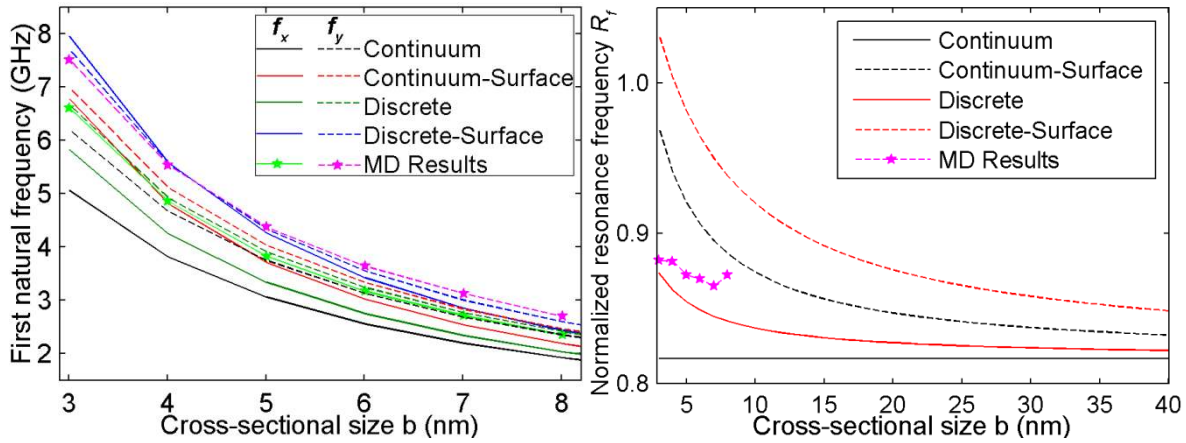


**FIG.11** (a) Comparison of the first natural frequencies between theoretical predictions and MD results. (b) Comparison of the normalized resonance frequency ( $R_f = f_x / f_y$ ) between theoretical predictions and MD results.